Damon CA, Gatley CM, Beres JJ, Finlay JA, Franco SC, Clare AS, Detty MR.
The performance of hybrid titania/silica-derived xerogels as active antifouling/fouling-release surfaces against the marine alga *Ulva linza*: *in situ* generation of hypohalous acids.
***Biofouling* 2016, 32(8), 883-896.**

The performance of hybrid titania/silica-derived xerogels as active antifouling/fouling-release surfaces against the marine alga *Ulva linza*: *in situ* generation of hypohalous acids

Corey A. Damon,[1] Caitlyn M. Gatley,[1] Joshua J. Beres,[1] John A. Finlay,[2] Sofia C. Franco,[2] Anthony S. Clare,[2] and Michael R. Detty[1*]

[1]Department of Chemistry, University at Buffalo, The State University of New York, Buffalo, New York 14260-3000, USA.

[2]School of Marine Science and Technology, Newcastle University, Newcastle NE1 7RU, UK

* For correspondence (mdetty@buffalo.edu)

Abstract: Mixed titania/silica xerogels were prepared using titanium tetraisopropoxide (TTIP) and tetraethoxy orthosilicate (TEOS). Xerogel properties were modified by incorporating *n*-octyltriethoxysilane (C8). The xerogels catalyze the oxidation of bromide and chloride with hydrogen peroxide (H_2O_2) to produce hypohalous acids at pH 7 and pH 8. The antifouling/ fouling-release performance of a TTIP/C8/TEOS xerogel in the presence and absence of H_2O_2 was evaluated for the settlement of zoospores of the marine alga *Ulva linza* and on the removal of 7-day-old sporeling biomass. In the absence of H_2O_2, differences in the settlement of zoospores and removal of sporelings were not significant relative to a titanium-free C8/TEOS xerogel. Addition of H_2O_2 gave a significant reduction in zoospore settlement and sporeling removal relative to the C8/TEOS xerogel and relative to peroxide-free conditions. The impact of TTIP on xerogel characteristics was evaluated by comprehensive contact angle analysis, scanning electron microscopy, and X-ray photoelectron spectroscopy.

Key Words: marine biofouling; xerogels; *Ulva linza*; antifouling; hydrogen peroxide; titanium oxide

Introduction

Marine biofouling is a continual problem for the shipping industry (Banerjee et al. 2011). Biofouling leads to an increase in roughness and drag on ships' hulls with subsequent loss of range and speed (Schultz 2007). Fuel consumption may account for up to 60% of a ship's operating costs and may increase by up to 40% in just six months on a ship without any treatment to minimize fouling (Schultz et al. 2011). Escalation in the production of greenhouse gases (through increased fuel consumption), corrosion, and the onset of cavitation also result from marine biofouling (Jack 1999; Atlar et al. 2011).

Antifouling (AF) paints containing metal complexes and/or biocides are currently used to combat marine biofouling, but raise concerns for environmental damage through leaching of metals or biocides (Borghi and Porte 2002; Chambers et al. 2006; Almeda et al. 2007). The recent development of fouling-release (FR) coatings to facilitate the removal of fouling organisms via water flow or cleaning, provides a more environmentally benign approach to reduce the effects of biofouling (Rosenhahn et al. 2010). FR technology largely relies on the use of silicone elastomers with low surface energy and modulus, properties that favor the release of fouling organisms (Baier et al. 1968; Pagliaro et al. 2009; Detty et al. 2014). The use of FR coatings to combat biofouling on immersed surfaces is limited by the fact that fouling is removed only in the presence of hydrodynamic shear or through regular cleaning (Lejars et al. 2012; Sokolova et al. 2012; Detty et al. 2014).

Coatings with the ability to generate materials *in situ*, either to discourage settlement or to minimize adhesion of biofouling organisms from reagents naturally present in seawater, represent one approach to combine the benefits of both AF and FR technologies (McMaster et al. 2009; Natalio et al. 2012; Ciriminna et al. 2015). The oxidation of halide salts with H_2O_2 found

in the aquatic environment can produce hypohalous acids *in situ*. The hypohalous acids have known biocidal effects (Williams and Schroeder 2004; Drabkova 2007) and discourage settlement of some species when generated *in situ* (McMaster et al. 2009; Natalio et al. 2012). Hydrogen peroxide thermodynamically can oxidize chloride, bromide, and iodide. For chloride and bromide, these reactions are kinetically slow (Mohammad and Liebhafsky 1934).

Hydrogen peroxide is found in the open ocean at concentrations up to 0.2 μM (Yuan and Shiller 2001) and can approach 50 μM in ports fed by rain water (Willey et al. 1999; Yuan and Shiller 2000) or by runoff (Clark et al. 2008). Hydrogen peroxide is also formed by photochemical decomposition of organic matter near the water surface (Cooper and Zika 1983) and can be produced by bacteria in the biofilm on submerged surfaces, approaching concentrations of 50 μM (Le Bozek et al. 2001). The ambient H_2O_2 can react with chloride (0.5 M), bromide (mM), and iodide (μM) present in seawater to produce low concentrations of hypohalous acid. The AF characteristics of a coating can be improved through the use of a coating-sequestered catalyst to activate H_2O_2 to increase the production of hypohalous acids at the surface generating a chemical deterrent for settlement of marine fouling organisms (McMaster et al. 2009; Natalio et al. 2012).

Sol-gel-derived xerogel coatings based on amorphous silica have shown promise as FR coatings (Sokolova et al. 2012; Sokolova et al. 2012a; Evariste et al. 2013) and have been modified to incorporate organochalcogenide catalysts for the activation of H_2O_2 (McMaster et al. 2009; Gatley et al. 2015). While they have shown some promise as AF coatings (McMaster et al. 2009), the FR characteristics of the surface are modified by the presence of the organochalcogen catalyst and FR characteristics may actually be reduced. Incorporating the catalytic site for activation of H_2O_2 as part of the inorganic matrix of the xerogel rather than in the organic

modifications imparting FR properties may lead to improved AF/FR characteristics of the surfaces.

The grafting of transition metals to mesoporous silica has provided an array of catalysts for the oxidation of halide salts with H_2O_2 (Walker et al. 1997). Oxidation of chloride with titanium grafted onto mesoporous silica was observed at pH 4 but not at pH 6.5 or higher, while oxidation of bromide with H_2O_2 was observed over the pH range 4-8. Oxidation of bromide with H_2O_2 has been observed with several grafted metals on silica in the reactivity order W > Mo > Ti > Zr > V > Re (Morey et al. 2000). Though the grafting of transition metals onto mesoporous silica does not present a practical approach to AF/FR coatings covering large surface areas, it does illustrate the potential of incorporating transition metal oxides into xerogel surfaces.

Herein, we describe the preparation of xerogel coatings via the sol-gel process that incorporate titanium tetraisopropoxide (TTIP) as part of the inorganic matrix and the AF/FR characteristics of these coatings toward zoospores and sporelings of the marine alga *Ulva linza*. The characterization of these surfaces by contact-angle analysis, scanning electron microscopy (SEM), and X-ray photoelectron spectroscopy (XPS) is also described. Importantly, the Ti-containing xerogels catalyze the oxidation of both chloride and bromide with H_2O_2 to produce the corresponding hypohalous acids at pH 8, which is the pH of seawater.

Materials and methods

Chemicals, Reagents, and Materials

Deionized (DI) water was prepared to a specific resistivity of at least 18 MΩ using a Barnstead NANOpure Diamond UV ultrapure water system. Tetraethoxy orthosilicate (TEOS) and *n*-octyltriethoxysilane (C8) were purchased from Gelest, Inc. and were used as received. Ethanol was purchased from Decon Laboratories. Hydrochloric acid, 2-propanol, and 30% hydrogen

peroxide were obtained from Fisher Scientific Co. Titanium tetraisopropoxide (TTIP) and 4-pentenoic acid were obtained from Acros Organics and were used as received. Deuterium oxide (>99%) was obtained from Cambridge Isotopes. Borosilicate glass microscope slides were obtained from Fisher Scientific, Inc.

The artificial seawater (ASW) used in chemical analysis was prepared via modification of the Marine Biological Laboratory (Woods Hole, Massachusetts, USA) recipe [Biological Bulletin Compendia: http://hermes.mbl.edu/BiologicalBulletin/COMPENDIUM/CompTab3.html#3A]. In addition to the salts used in the MBL recipe, 1.0 mM of sodium bromide and 1.0 µM of sodium iodide were added to give a more realistic representation of the halide ions present in natural seawater. For algal assays, artificial seawater (ASW) was made from Tropic Marin® salts.

Xerogel composition

Xerogel monoliths were prepared at room temperature. A TEOS monolith was prepared by mixing TEOS (10.0 mmol, 2.23 ml) and EtOH (10.4 mmol, 607 µl) in a glass vial while stirring. Water (13.5 mmol, 243 µl) and HCl (24.6 µl of a 1.0 M solution) were combined in a separate vial and added dropwise to the reaction mixture with stirring. Following addition of acid, the monolith was left stirring open to the atmosphere, at ambient temperature until gel formation was observed and all solvent had evaporated. The xerogel was then dried under reduced pressure for 48 h at ambient temperature, and then crushed using mortar and pestle.

The TTIP/TEOS monolith was prepared following the TEOS protocol using TTIP (2.00 mmol, 0.592 ml) and TEOS (8.00 mmol, 1.79 ml) in the initial step (20:80 molar ratio of TTIP to TEOS). The C8/TEOS monolith was prepared following the TEOS protocol using C8 (4.00 mmol, 1.26 ml) and TEOS (6.00 mmol, 1.34 ml; a 40:60 molar ratio of TTIP to TEOS). The

TTIP/C8/TEOS monolith was prepared following the TEOS protocol using TTIP (2.00 mmol, 0.592 ml), C8 (4.00 mmol, 1.26 ml) and TEOS (4.00 mmol, 893 µl; a 20:40:40 molar ratio of TTIP, C8, and TEOS).

Sols for spin coating were prepared at ambient temperature. A TEOS sol was prepared from H_2O (8.00 mmol, 144 µl) and acetic acid (4.00 mmol, 229 µl) in isopropanol (7.96 mL) and adding this solution dropwise to stirring TEOS (4.46 mL, 20.0 mmol). The resulting sol was capped and stirred for 24 h prior to coating. The TTIP/TEOS sol was prepared following the TEOS protocol using TTIP (4.00 mmol, 1.18 ml) and TEOS (16.0 mmol, 3.57 ml). The C8/TEOS sol was prepared following the TEOS protocol using C8 (8.00 mmol, 2.53 ml) and TEOS (12.0 mmol, 2.68 ml). The TTIP/C8/TEOS sol was prepared following the TEOS protocol using TTIP (4.00 mmol, 1.18 ml), C8 (8.00 mmol, 2.53 ml), and TEOS (8.00 mmol, 1.79 ml).

Xerogel films were formed as described by Bennett et al. (2010) by spin-casting 400 µl of the sol precursor onto pre-cleaned 25 mm × 75 mm glass microscope slides. Slides were cleaned by soaking in 'piranha solution' (1:4 30% H_2O_2: concentrated H_2SO_4) for 24 h, rinsed with copious quantities of DI water, soaked in isopropanol for at least 15 min, and were air dried immediately prior to coating. A spin coater [Specialty Coating Systems, Inc., model P6700] was used at 100 rpm for 10 s to deliver the sol and at 3000 rpm for 30 s to coat. All coated surfaces were dried at ambient temperature for at least seven days prior to analysis of the surface properties.

Characteristics of xerogel coatings: contact angles and surface energies pre- and post-immersion

Xerogel films were stored in air prior to measurement of static contact angles for the surface. Slides were then immersed in ASW for 24 h followed by 1 h in DI water to remove salts. The coatings were then allowed to dry under ambient conditions for 3 h before contact angles were

remeasured. Static water contact angles (θ_{Ws}) and static diiodomethane contact angles [$\theta_{(CH2I2)s}$] were measured on a 15 μl drop of fluid on the xerogel surface with a contact angle goniometer [ramé-hart, Model NRL 100]; both sides of the droplet profile were measured. Contact angles measured with water and diiodomethane were treated as described by Owens and Wendt (1969) to give total surface energy (Baier and Meyer 1992) as compiled in Table 1.

Characteristics of xerogel coatings: scanning electron microscopy (SEM)

Scanning electron micrographs were recorded using an Hitachi model SU-70 field emission-SEM with a zirconium oxide/tungsten Schottky electron emission source operating at 5 kV acceleration voltage, three state electromagnetic lens system, octapole electromagnetic type stigmator coil, two-state electromagnetic deflection type scanning coil, Everhart Thornly secondary electron detectors, and SEM Data Manager software 1.0.

Characteristics of xerogel coatings: X-ray photoelectron spectroscopy pre- and post-immersion

The xerogel coatings were also examined by X-ray photoelectron spectroscopy (XPS), pre- and post-immersion in DI water or 200 μM H_2O_2 (Tang et al. 2005; McMaster et al. 2009; Gatley et al. 2015) using a Physical Electronics Laboratories (PHI) Model 500 VersaProbe equipped with an Aluminum X-Ray source, a hemispherical analyzer and a 16 channel detector. A monochromatic Al kα^2 source (1486.6eV) was operated at 100 μm 25 W 15 kV with a 45° takeoff angle at a pressure not exceeding 5×10^{-6} Pa in the main chamber. Pass energies of 117.4 eV and 25.30 eV were used to obtain survey and high-resolution multiregion scans, respectively. Curve fitting was performed with PHI MultiPak™ Software Version 8.

A coated slide was cut into 1 cm × 1 cm samples using a diamond-tipped glass cutter. Initial analysis of the coating was performed on a dry sample that had been stored open to air. After dry analysis, the same sample was submersed for 24 h in DI water or in DI water with 200 μM

H_2O_2. Following the soaking procedure, the sample was rinsed in DI water and air-dried at ambient conditions for 15 h to ensure all water had evaporated off the coating prior to introduction to the high vacuum chamber of the instrument. While the air-drying step of the pretreatment may reverse changes to the coating caused by immersion, a dry coating is required for the high vacuum conditions of XPS. The composition of the surface, which is dry but previously immersed, corresponds to a kinetically trapped condition rather than the thermodynamic equilibrium state when in contact with water, as the recovery from immersion is slow for xerogel films (Martinelli et al. 2008; Evariste et al. 2013).

Kinetic Studies of halogenation reactions with xerogel monoliths

The halogenation of 4-pentenoic acid was monitored by ^{1}H NMR spectroscopy using previously described techniques (Alberto et al. 2015; Gatley et al. 2015). Briefly, a stock solution of pH 7.0 buffer was prepared from a 0.72:1 molar ratio of K_2HPO_4/KH_2PO_4 (0.23 M in total phosphate) was prepared in D_2O with propionic acid (0.01 M) as an internal standard. A pH 8.0 buffer was prepared from a 0.14:1 molar ratio of K_2HPO_4/KH_2PO_4 (0.23 M in total phosphate) with final pH adjusted using 3 M NaOH. For brominations, NaBr (7.5 mmol, 1.4 M final concentration), and 4-pentenoic acid (**1**, 0.075 g, 0.75 mmol, 0.14 M final concentration), were added to 5.0 mL of the stock solution of pH 7.0 buffer followed by the xerogel monolith [8.7 mg of either the TTIP/TEOS monolith (0.027 mmol Ti, 0.035 equiv based on total Ti relative to substrate) or the TEOS monolith or 11.5 mg of the TTIP/C8/TEOS (0.027 mmol Ti, 0.035 equiv based on total Ti relative to substrate), TEOS, or the C8/TEOS monolith]. The H_2O_2 (0.26 mL of a 4.4 M aqueous solution, 1.1 mmol, 0.21 M final concentration) was added and the reaction vessels were placed in a thermostat-controlled bath at 298 ± 1 K.

For chlorinations, the process was repeated with NaCl (15 mmol, 2.7 M final concentration), 4-pentenoic acid (**1**, 0.075 g, 0.75 mmol, 0.14 M), and 5.0 mL of the stock solution of pH 7.0 KH_2PO_4 or pH 8.0 buffer. The xerogel monolith [0.15 g of the TTIP/TEOS monolith (0.45 mmol Ti) or the TEOS monolith or 0.23 g of the TTIP/C8/TEOS (0.45 mmol Ti), TEOS, or the C8/TEOS monolith] was added followed by H_2O_2 (0.43 mL of an 8.8 M solution, 3.8 mmol, 0.68 M). The reaction vessels were placed in a thermostat-controlled bath at 298 ± 1 K.

Reaction mixtures were periodically sampled by ^{1}H NMR spectroscopy with suppression of H_2O and DOH signals. Consumption of 4-pentenoic acid was determined from the relative integral values of the internal alkene proton of 4-pentenoic acid (δ = 5.8 ppm) and the methylene protons of propionic acid (δ = 1.1 ppm). The experiments were followed through the one to three half-lives and results plotted assuming pseudo-first order conditions [n [4-pentenoic acid] vs. time (s)]. NMR spectra were recorded on an Inova 500 (500 MHz for ^{1}H) or Inova 300 instrument (300 MHz for ^{1}H).

Bromination of 4-pentenoic acid (**1**) gave 5-(bromomethyl)dihydrofuran-2(3H)-one (**3a**, Scheme 1) with spectral characteristics matching those previously reported (Alberto et al. 2015, Gatley et al. 2015). Chlorination of **1** gave 5-(chloromethyl)dihydrofuran-2(3H)-one (**3b**, Scheme 1) with spectral characteristics matching those previously reported (Genovese et al. 2010).

Kinetic studies of halogenation reactions on xerogel-coated glass cuvettes

A 1 cm × 1 cm glass cuvette was cleaned by soaking in 'piranha solution' (1:4 30% H_2O_2: concentrated H_2SO_4) for 24 h, rinsing with copious quantities of DI water, soaking in isopropanol for 3 h, and drying in air. A xerogel film was then applied to one side of the cuvette

by administering 1.0 ml of the 20:40:40 TTIP:C8:TEOS sol for 60 s, after which the remaining sol was removed. The 'coated cuvette' was dried at ambient temperature for 5 days prior to use.

The halogenation of phenol red was monitored by UV-Vis spectroscopy in the coated cuvette. Phenol red (0.15 μmol, 50 μM final concentration) and H_2O_2 (0.15 μmol, 50 μM final concentration) were added to 2.8 ml of artificial seawater (0.5 M in chloride, 1.0 mM in bromide, and 1.0 μM in iodide at pH 8) in the coated cuvette. Halogenation of phenol red was monitored over a 24-h period at 298 ± 1 K. The chlorination of phenol red was followed via the incremental addition of chlorine bleach (HOCl) to give the equivalent of 10, 15, 25, 50, 75, 100, and 200 μM HOCl.

Biological Assays

***Settlement of zoospores of* Ulva linza**

Fronds of *U. linza* were collected from Craster, Northumberland, UK (55° 26' N; 1° 35' W) and a spore suspension of 1.0×10^6 spores mL^{-1} was prepared by the method of Callow et al. (1997). The experiment used 3 replicates of each coating for each treatment. All coatings were equilibrated in 0.22 μm-filtered ASW with added H_2O_2 (0, 50, 100 and 150 μM), depending on the treatment, for 24 h prior to testing. A suspension of zoospores (10 mL; 1×10^6 spores mL^{-1}) was added to individual compartments of quadriPERM® dishes containing the samples. After 45 min in darkness at 20 °C, the slides were washed by passing 10× through a beaker of seawater to remove unsettled (i.e. swimming) spores. Slides were fixed using 2.5% glutaraldehyde in seawater. The density of zoospores attached to the surface was counted on each of 3 replicate slides using an image analysis system attached to a Zeiss Axioscope 2 plus fluorescence microscope. Spores were visualized by autofluorescence of chlorophyll. Counts were made using Axiovision 4 software for 30 fields of view (0.15 mm^2) on each slide.

Settlement of zoospores of* U. linza *in the presence of sodium hypochlorite

Reagent grade sodium hypochlorite solution was purchased from Sigma: (Sigma 425044-250ML-D). The solution contained available chlorine at 10-15%. Molar concentrations were calculated on the basis of 12.5% chlorine. The sodium hypochlorite solution was diluted in ASW to produce a range of dilutions in 24-well plates, to which spores were added (suspension of 3.33 x 10^5 spore ml^{-1}). After 45 min in darkness at c. 20 °C, the wells were washed to remove unsettled (i.e. swimming) spores by emptying and refilling with filtered ASW twice. Wells were fixed using 2.5% glutaraldehyde in seawater and the density of zoospores attached to the surface was counted on each of 4 replicate wells using the image analysis system as described above. Spores were visualized by autofluorescence of chlorophyll. Counts were made using Axiovision 4 software for 10 fields of view (0.15 mm^2) on each slide. EC_{50} values were determined by graphical interpolation.

***Growth and attachment of sporelings of* U. linza**

Spores were allowed to settle on 6 coated slides for 45 min and then washed as described above. Spores were cultured using enriched seawater medium (Starr and Zeikus 1987) for 7 days to produce sporelings (young plants). Sporeling growth medium was refreshed every 48 h along with H_2O_2 as appropriate. Sporeling biomass was determined *in situ* by measuring the fluorescence of the chlorophyll contained within the sporelings in a Tecan fluorescence plate reader. The relative fluorescence unit (RFU) value for each slide was derived from the mean of 70 point fluorescence readings taken from the central portion of each slide. The strength of attachment of sporelings was assessed using an impact pressure of 30 kPa from a water jet (Aldred et al. 2010). Biomass remaining was determined using the fluorescence plate reader (as

above). Percentage removal was calculated from readings taken before and after exposure to the water jet.

Growth of sporelings of U. linza *in the presence of sodium hypochlorite*

The sodium hypochlorite solution was diluted in seawater (nutrient supplemented) to produce a range of dilutions in 24-well plates, to which spores were added (suspension of 3.33×10^5 spore ml^{-1}). Four replicate wells of each concentration were prepared. The plates were incubated for 7 d in an illuminated chamber at 18 °C. Biomass was quantified as chlorophyll, which was extracted in dimethyl sulfoxide (DMSO). Plates were then incubated in darkness for 1 h to ensure the chlorophyll in the sporelings had been extracted. The fluorescence of the samples was read in a Tecan fluorescence plate reader. EC_{50} values were determined by graphical interpolation.

Data analysis and statistics

For biological assays on coated slides, statistical significance was assessed using one-way ANOVA and a post-hoc multiple pairwise comparison using the Tukey test with a significance level of 0.05. The Student's t-test was used for pair-wise comparisons of independent samples with respect to physicochemical characteristics of surfaces with one nominal variable and one measurement variable. A p value <0.05 was considered significant.

Results

Characterization of surfaces: appearance and optical transparency

TEOS, TTIP/TEOS, C8/TEOS and TTIP/C8/TEOS sols were cast via spin-coating onto glass slides to give colorless, transparent coatings. Sols can also be applied to larger surfaces via dip-coating or brushing. Surfaces are uniform in appearance via all modes of coating.

Characterization of surfaces: contact angles and surface energies

Static water contact angles, $\theta_{Ws}°$ and static diiodomethane contact angles, $\theta_{(CH2I2)s}°$ (Table 1) were measured for all xerogel surfaces described in this study pre- and post-immersion in ASW. Contact angles measured with water and diiodomethane were treated as described by Owens and Wendt (1969) to give total surface energy (γ_S) (Baier and Meyer 1992) for the xerogel surfaces of this study pre- and post-immersion in ASW (Table 1).

Prior to immersion, the TEOS and the TTIP/TEOS xerogel coatings had comparable values of $\theta_{Ws}°$, (44° and 45°, respectively, Table 1) and γ_S (56 and 57 mN m^{-1}, respectively) that were not significantly different to each other ($p = 0.72$ and $p = 0.57$, respectively). Post immersion, values of $\theta_{Ws}°$ (31° and 35°, respectively) decreased significantly ($p < 0.0001$ and $p = 0.0015$, respectively) and values of γ_S (63.9 and 62.1 mN m^{-1}, respectively) increased significantly ($p = 0.0028$ and $p = 0.038$, respectively) from pre-immersion values. However, comparing these values for both surfaces post immersion indicated that differences between the two surfaces were not significant ($p = 0.17$ for $\theta_{Ws}°$ and $p = 0.19$ for γ_S).

The C8/TEOS xerogel coating and the TTIP/C8/TEOS xerogel coating had comparable values of $\theta_{Ws}°$ (102.8° and 99.1°, respectively) and γ_S (23.2 and 25.0 mN m^{-1}, respectively) pre-immersion in ASW (Table 1). These differences in γ_S, though small, were significant (Student's t-test, $p = 0.0002$) Following immersion, values of $\theta_{Ws}°$ (99.4° and 94.1° for the C8/TEOS and the TTIP/C8/TEOS xerogels, respectively) decreased significantly ($p < 0.0001$ and $p = 0.0003$, respectively) and values of γ_S (26 and 27 mN m^{-1}, respectively) increased significantly ($p = 0.0089$ and $p = 0.026$, respectively) from pre-immersion values (Table 1). Post immersion, values of γ_S were not significantly different ($p = 0.29$) for the two surfaces.

Characterization of surfaces: scanning electron microscopy (SEM)

Figure 1 depicts typical SEM images for the TTIP/C8/TEOS xerogel viewed from the top and along an edge pre- and post-immersion in ASW. Pre-immersion images were obtained from xerogel surfaces stored in air for one week following coating. Post-immersion images were obtained from xerogel surfaces immersed in ASW for 7 d followed by a rinse with DI water. The xerogel surfaces are smooth and uncracked both pre- and post-immersion. The view along the edge shows that the surfaces are approximately 0.5 μm thick.

Characterization of surfaces: X-ray photoelectron spectroscopy (XPS)

XPS spectra of the TTIP/C8/TEOS xerogel surfaces were recorded at a take-off angle of 45° to determine atomic composition at the surface of the xerogel coating pre- and post-immersion for 24 h in DI water or for 24 h in 200 μM H_2O_2. Results are shown in Figure 2 as elemental ratios for the C(1s)/Si(2p3), C(1s)/Ti(2p), and Si(2p3)/Ti(2p) signals as determined by area under the peaks corrected for relative sensitivity factors. In clean borosilicate glass, the ratio of the C(1s)/Si(2p3) signals is 0.28 ± 0.02, which is quite similar to the ratio of 0.2 reported by Tang et al. (2005), suggesting a relatively carbon-free surface with any carbon found presumably arising from adventitious/adsorbed carbon-containing species from the atmosphere.

The elemental ratios shown in Figure 2 are not significantly different pre- and post-immersion in either DI water or 200 μM H_2O_2 (Student's t-test, $p > 0.05$). These data suggest that neither immersion in water nor exposure to aqueous peroxide results in significant changes to the surface structure with respect to C, Si, and Ti.

Oxidation of bromide with H_2O_2 catalyzed by xerogel monoliths

For the TTIP/TEOS and TTIP/C8/TEOS xerogel coatings to have active AF characteristics, the coatings should oxidize halide salts in the presence of H_2O_2. The 20:80 TTIP/TEOS and 20:40:40 TTIP/C8/TEOS monoliths were prepared and ground into a fine powder using a mortar

and pestle. For comparison, Ti-free TEOS-only and C8/TEOS monoliths were prepared and were similarly ground into a fine powder. The ability of these four monoliths to catalyze the halogenation of 4-pentenoic acid (**1**) to give 4,5-dihalopentanoic acids **2** and/or 5-(halomethyl)dihydrofuran-2(3H)-ones **3** (Scheme 1) with H_2O_2 and either NaBr or NaCl was examined. 4-Pentenoic acid has been used as a reporter molecule in several studies because of its very rapid reaction with hypohalous acids (Goodman & Detty 2004, Bennett et al. 2008, Alberto et al. 2015, Gatley et al. 2015).

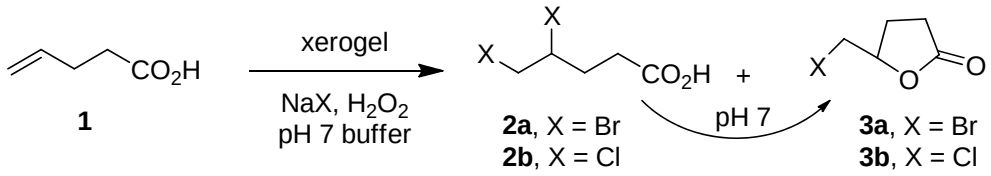

Scheme 1. Halogenation of 4-pentenoic acid (**1**) with hypobromous or hypochlorous acid.

Bromination of **1** at pH 7 and 298 ± 1 K with 1.4 M NaBr and 0.21 M H_2O_2 with the TTIP/TEOS or TTIP/C8/TEOS monoliths (3.5 mole-% Ti relative to **1**) or an equivalent weight of the TEOS or C8/TEOS monoliths was followed by ^{1}H NMR spectroscopy. The loss of **1** was followed as well as the appearance of a mixture of 4,5-dibromopentanoic acid (**2a**) and bromolactone **3a**. The ^{1}H NMR chemical shifts of the olefinic protons of **1** are distinct from the bromomethine proton of **2a** and the lactone methine proton of **3a**. At pH 7 or higher, **2a** is converted to **3a** upon standing. Rate constants, k_{obs}, for loss (or bromination) of **1** are compiled in Table 2. As shown in Figure 3a for the TEOS-only, TTIP/TEOS, and TTIP/C8/TEOS xerogels, pseudo-first-order behavior was observed for the loss of **1** with concomitant formation of **2a** and **3a**. Bromination with the TTIP/TEOS xerogel [k_{obs}, = (8.44 ± 0.10) × 10^{-5} s^{-1}] was 340-fold faster than bromination with the Ti-free, TEOS-only xerogel [k_{obs} of (2.47 ± 0.15) × 10^{-7}] while

bromination with the TTIP/C8/TEOS xerogel [k_{obs} = (3.37 ± 0.09) × 10^{-6} s^{-1}] was 14-fold faster (Table 2).

As shown in Figure 4b, TTIP/C8/TEOS catalyzed the oxidation of bromide with H_2O_2 at pH 8. The rate was 2-fold faster at pH 8 than the control reaction with the TEOS monolith as catalyst (Table 3).

Oxidation of chloride with H_2O_2 catalyzed by xerogel monoliths

Oxidation of chloride was slower at 298 ± 1 K and utilized higher concentrations of halide (2.7 M NaCl) and H_2O_2 (0.68 M) and a 60 mole-% in Ti loading of the TTIP/TEOS and TTIP/C8/TEOS xerogels. As shown in Figure 3c, pseudo-first-order behavior was observed for the loss of **1** with concomitant formation of **2b** and **3b** in the presence of TEOS-only, TTIP/TEOS, and TTIP/C8/TEOS xerogels. Chlorination with the TTIP/TEOS xerogel [k_{obs}, = (1.51 ± 0.05) × 10^{-5} s^{-1}] was 100-fold faster than chlorination with the Ti-free, TEOS-only xerogel [k_{obs} of (1.89 ± 0.68) × 10^{-7}] while chlorination with the TTIP/C8/TEOS xerogel [k_{obs} = (3.37 ± 0.09) × 10^{-6} s^{-1}] was 22-fold faster (Table 2). An intermediate level of the TTIP/C8/TEOS monolith (20 mole-% Ti relative to **1**) gave k_{obs} for chlorination of **1** of (1.03 ± 0.05) × 10^{-6} s^{-1} (Table 2).

As shown in Figure 3d, the TTIP/C8/TEOS xerogel catalyzed the chlorination of **1** with NaCl (2.7 M) and H_2O_2 (0.68 M) at pH 8.0. The Ti-containing xerogel gave a 20-fold increase in rate relative to the Ti-free TEOS xerogel.

Oxidation of halide salts with H_2O_2 in ASW

The halogenation of 4-pentenoic acid (**1**) at 298 ± 1 K in ASW (pH 8) containing 0.5 M chloride, 1.0 mM bromide, 1.0 μM iodide and 50 μM H_2O_2 was monitored by ^{1}H NMR spectroscopy. The reaction vessel was a glass cuvette coated on one internal face with the

TTIP/C8/TEOS xerogel. After 5 days, no loss of **1** was observed and no halogenation products of **1** were detected.

The halogenation of phenol red, which has been used to monitor the oxidation of halide salts with H_2O_2 (Walker et al. 1997), was also examined. Incremental addition of bleach (HOCl) to give the equivalent of 10, 15, 25, 50, 75, 100, and 200 μM HOCl to phenol red (50 μM) at 298 ± 1 K in ASW (pH 8) was monitored spectrophotometrically as shown in Figure 4a. An expansion of the 400-450-nm region is shown in Figure 4b for 0, 10, 15, and 25 μM HOCl. The halogenation of phenol red (50 μM) at 298 ± 1 K in ASW (pH 8) containing 50 μM H_2O_2 was monitored spectrophotometrically in the glass cuvette coated on one internal face with the TTIP/C8/TEOS xerogel. After 24 h, minimal halogenation of phenol red was observed (Figures 4b and 4c).

***Settlement of zoospores of* U. linza**

The 50:50 C8/TEOS xerogel, used as a control xerogel surface in previous studies (Bennett et al. 2010; Gunari et al. 2011; Sokolova et al. 2012; Sokolova et al. 2012a), and the 20:40:40 TTIP/C8/TEOS xerogel were soaked in either ASW, or in ASW with different concentrations of H_2O_2 for 24 h prior to settlement of zoospores of *U. linza*. Spore settlement data on these surfaces are shown in Figure 5. One-way analysis of variance indicated that there were significant differences within the data set ($F_{5, 534} = 157$ $P < 0.001$). A post-hoc Tukey test showed there was no significant difference in spore settlement between the control 50:50 C8/TEOS xerogel surface and the 20/40/40 TTIP/C8/TEOS xerogel surface in the absence of H_2O_2 ($p = 0.073$). However, at 50 and 100μM H_2O_2, spore settlement densities on the TTIP/C8/TEOS xerogel surface were significantly reduced relative to the C8/TEOS surface. The addition of 50 μM H_2O_2 gave an 11% decrease in mean settlement on the C8/TEOS coating, but

a 53% decrease in mean settlement on the TTIP/C8/TEOS coating ($p < 0.001$). The addition of 100 μM H_2O_2 gave a 17% decrease in settlement on the C8/TEOS coating and a 56% decrease in settlement on the TTIP/C8/TEOS coating ($p < 0.001$).

***Growth and attachment of sporelings of* U. linza**

Sporelings grew well on all surfaces in ASW and in ASW supplemented with 50 μM and 100 μM H_2O_2. A green covering was visible on all surfaces after seven days. One-way analysis of variance ($F_{5, 30} = 12.2$ $P < 0.001$) and Tukey test showed that, there was no significant difference in sporeling biomass on the C8/TEOS and TTIP/C8/TEOS coatings in the absence of H_2O_2 ($p = 0.99$, Figure 6a). The addition of 50 μM H_2O_2 had no significant impact on sporeling biomass on the C8/TEOS control ($p = 0.95$). However, the addition of 50 μM H_2O_2 caused significant removal of sporeling biomass on the TTIP/C8/TEOS xerogel compared to the C8/TEOS xerogel ($p = 0.04$). The presence of 100 μM H_2O_2 caused a further decrease in sporeling biomass on both control and TTIP surfaces, but the final quantities were not significantly different from each other ($p = 0.11$).

The strength of attachment of 7-day-old sporelings was assessed using an impact pressure of 30 kPa from a water jet (Figure 6b). One-way analysis of variance $F_{5, 30} = 6.7$ $P < 0.001$ and Tukey test showed there was no significant difference in the percentage of sporeling biomass removed from the C8/TEOS control and TTIP/C8/TEOS xerogel in the absence of H_2O_2 ($p = 1.00$) However, the addition of 50 μM H_2O_2 caused a significant increase in the removal of sporeling biomass from the TTIP/C8/TEOS xerogel (50.2%) than from the C8/TEOS control coating (23.9%, $p = 0.0011$). With 100 μM H_2O_2, there was an increase in removal from the C8/TEOS coating resulting in no significant difference between it and TTIP/C8/TEOS xerogel ($p = 0.99$), which suggested that H_2O_2 alone was impacting the strength of adhesion.

Settlement of zoospores of* U. linza *in the presence of sodium hypochlorite

Zoospores of *U. linza* were added to sodium hypochlorite diluted in seawater to produce a range of concentrations in 24-well polystyrene plates. Spore settlement data on polystyrene at each concentration are shown in Figure 7a. An EC_{50} value for 50% inhibition of zoospore settlement was observed at ≈150 μM sodium hypochlorite.

Growth of sporelings of* U. linza *in the presence of sodium hypochlorite

Zoospores of *U. linza* were added to sodium hypochlorite diluted in seawater to produce a range of concentrations in 24-well polystyrene plates. The plates were incubated for 7 d and sporeling biomass was quantified as chlorophyll as shown in Figure 7b. A concentration of ≈200 μM sodium hypochlorite in seawater inhibited sporeling growth by 50%.

Discussion

Sol-gel processed, xerogel materials are readily prepared by the hydrolysis of metal or semi-metal alkoxides to give surfaces with tunable characteristics, such as surface functionality, surface area, surface wettability, and surface energy (Brinker & Scherer, 1990; Avnir, 1995; Dave et al. 1995; Ingersoll & Bright, 1997). The xerogels of this study incorporate mixed titanium and silicon oxides in order to introduce titanium oxide as a catalyst for the activation of H_2O_2 in the inorganic matrix of the xerogel coating. Both the inorganic TTIP/TEOS and organically-modified TTIP/C8/TEOS xerogels, when used as crushed monoliths, accelerated the production of hypohalous acids from either sodium bromide or sodium chloride with H_2O_2 (Table 2 and Figure 3), as measured by the halogenation of 4-pentenoic acid (**1**, Scheme 1), and have the potential to be active AF surfaces. Oxidation of chloride with H_2O_2 via a xerogel-sequestered catalyst has not been previously observed. Oxidation of chloride with H_2O_2 has

been observed with transition metals grafted onto mesoporous silica, but these reactions failed at pH 6.5 or higher (Walker et al. 1997). Oxidation of chloride with H_2O_2 was observed with the TTIP/C8/TEOS xerogel at pH 7.0 and at pH 8.0.

The FR characteristics of xerogel coatings have been improved previously by incorporation of organically-modified trialkoxysilanes into the xerogel framework (Sokolova et al. 2012; Sokolova et al. 2012a; Evariste et al. 2013; Detty et al. 2014). The 50:50 C8/TEOS xerogel has shown FR characteristics with juvenile barnacles, algal sporelings, and microalgae (Tang et al. 2005; Sokolova et al. 2012). The performance of FR coatings is influenced by the inherent surface energy (γ_s) of the coating. For biofouling applications, γ_S describes the mechanical work necessary to overcome an organism's adhesion to the surface. In doing so, a new surface is created, and γ_S defines the energy required to create a new unit area of surface (mN m^{-1}). The incorporation of C8 into the xerogel formulations lowers γ_s for the coating.

Replacing TEOS in the xerogel formulations with 20 mole-% TTIP actually has minimal impact on relative values of γ_S in comparisons of the TEOS-only and TTIP/TEOS or C8/TEOS and TTIP/C8/TEOS coatings. For the TEOS-only and TTIP/TEOS coatings, replacing TEOS with 20 mole-% TTIP in the xerogel formulation gave no statistically significant difference between the two surfaces with respect to γ_S before and after immersion in ASW (Table 1). Pre-immersion in ASW, replacing TEOS in the C8/TEOS coating with 20 mole-% TTIP in the TTIP/C8/TEOS coating gave a small but significant increase in γ_S (23.2 ± 0.2 mN m^{-1} and 25.0 ± 0.1 mN m^{-1}, respectively). However, following immersion in ASW, replacing TEOS with 20 mole-% TTIP had no significant impact on γ_S (26 ± 1 mN m^{-1} and 27 ± 1 mN m^{-1}, respectively, Table 1).

The TTIP/C8/TEOS coating is colorless and transparent while the scanning electron micrographs of Figure 2 show that the surface is smooth and uncracked – even after 7 days of immersion in ASW. The SEM images of this surface appear quite similar to those reported for the 50:50 C8/TEOS surface (Tang et al. 2005) and again indicate that the substitution of TTIP for TEOS in the xerogel formulations has minimal impact on surface characteristics.

The AF characteristics of the xerogel surface can be improved by replacing TEOS in the xerogel formulation with 20 mole-% TTIP. In the absence of H_2O_2, no significant difference was observed in the settlement of zoospores of *U. linza* on the C8/TEOS xerogel control or on the TTIP/C8/TEOS xerogel surface (Figure 5). In the presence of 50 μM H_2O_2, mean zoospore settlement was greatly reduced on the TTIP/C8/TEOS coating (53%) relative to the C8/TEOS coating (11%, Figure 5). The difference in settlement between the two surfaces suggests that H_2O_2 activates the Ti-catalyst, which then discourages settlement of zoospores of U. linza via the oxidation of halide salts on the coating surface to hypohalous acids. Increasing the H_2O_2 concentration to 100 μM gave a slight additional reduction in settlement on both surfaces.

The halogenation of **1** shown in Figure 3 used concentrations of bromide and chloride much higher than those found in seawater and concentrations of H_2O_2 1000-fold greater than the 50 μM H_2O_2 used to discourage zoospore settlement in Figure 5. The lack of halogenation products from **1** under conditions that discouraged settlement of zoospores of *U. linza* suggest that hypohalous acids are not being produced in high concentrations in the bulk solution.

Some boundaries for hypohalous acid production by the TTIP/C8/TEOS xerogel surface can be established from the halogenation of phenol red (Figure 4). The inset of Figure 4a is a plot of the absorbance at 434 nm following the addition of incremental amounts of HOCl to phenol red. The slope of that line is 2.31×10^{-3} absorbance units per μM bleach. Comparing Figure 4b with

Figure 4c, the amount of bleach produced is equivalent to ≤ 5 μM for an initial concentration of bleach (or ≤ 0.2 nmol/mL/h of bleach produced in the coated cuvette). The data shown in Figure 7a give an EC_{50} of ≈150 μM for a 50% reduction of zoospore settlement and an EC_{50} of ≈200 μM for a 50% reduction in sporeling biomass. These results suggests that bulk hypohalous acid is not responsible for the reduction in zoospore settlement shown in Figure 5. Peroxide activation of Ti to a peroxotitanium(IV) species (Walker et al. 1997) and interaction of that species with halide can present a surface with a high oxidizing potential to discourage zoospore settlement.

Following zoospore settlement, there was no significant difference in 7-day-old sporeling biomass on the TTIP/C8/TEOS surfaces relative to the C8/TEOS control. In the presence of 50 μM hydrogen peroxide, less sporeling biomass was present on the TTIP/C8/TEOS surfaces relative to the C8/TEOS control, which may simply reflect the reduced settlement of zoospores on the TTIP/C8/TEOS surfaces. At 100 μM hydrogen peroxide, the difference between the TTIP/C8/TEOS surface and the C8/TEOS control, while still significant, was reduced.

Enhanced FR characteristics in the presence of H_2O_2 were observed on the TTIP/C8/TEOS surface relative to the C8/TEOS surface. In the absence of H_2O_2, no significant difference in the removal of 7-day old sporelings was observed in comparing the C8/TEOS and TTIP/C8/TEOS coatings (32% removal from each, Figure 6). However, the removal of sporelings cultured in the presence of 50 μM hydrogen peroxide was significantly greater from the TTIP/C8/TEOS coatings (52% removal) than from the control C8/TEOS coatings (23% removal). At 100 μM H_2O_2, there was no longer a significant difference in the removal of sporeling biomass between the two surfaces (45-50% removal). The latter observation suggests that high concentrations of H_2O_2 alone can impact adhesion.

In conclusion, replacing TEOS in silica-derived xerogels with TTIP can provide "active" xerogel surfaces that use reagents found in seawater (H_2O_2, 0.5 M chloride, 1 mM bromide, and 1 μM iodide) to reduce settlement of zoospores of *U. linza*. The "active" xerogel surface provides a chemical deterrent to the settlement of zoospores of *U. linza* and reduces the strength of adhesion of sporelings to the surface in the presence of 50 μM H_2O_2. This concentration of H_2O_2 can occur naturally under some conditions in the marine environment (Willey et al. 1999; Yuan and Shiller 2000; Le Bozek et al. 2001; Clark et al. 2008). Importantly, the titania/silica hybrid xerogels are the first to catalyze the oxidation of chloride with H_2O_2 and the oxidation of chloride occurs at pH 7.0 and pH 8.0. In seawater, the 500-fold higher concentration of chloride relative to bromide provides a kinetic advantage for the oxidation of chloride.

The findings of this study indicate that replacing TEOS with TTIP in the xerogel formulations has minimal impact on xerogel surface characteristics and that the mixed titania/silica xerogels remain transparent and applicable via a variety of coating techniques. The AF and FR characteristics are observed at pH 8 – the pH of seawater. This approach can be extended to balance AF and FR properties through the use of different loading levels of TTIP, as well as the use of different transition metal oxides (Morey et al. 2000), and through the use of different organo(trialkoxy)silanes for the coating matrix (Gunari et al. 2011; Sokolova et al. 2012; Sokolova et al. 2012a; Evariste et al. 2013).

Acknowledgements

SF/JAF/ASC (awards N00014-13-1-0633 and N00014-13-1-0634) and CAD/CMG/MRD (awards N00014-15-1-2400 and N00014-13-1-0430) thank the U. S. Office of Naval Research for partial support of these studies.

References

Alberto EE, Muller LM, Detty MR. 2015. Rate acceleration of bromination reactions with NaBr and H_2O_2 via the addition of catalytic quantities of diaryl ditellurides. Organometallics. 33: 5571-5581.

Aldred N, Scardino A, Cavaco A, de Nys R, Clare AS. 2010. Attachment strength is a key factor in the selection of surfaces by barnacle cyprids (*Balanus amphitrite*) during settlement. Biofouling. 26: 287-299.

Almeida E, Diamantino TC, De Sousa O. 2007. Marine paints: The particular case of antifouling paints. Prog Org Coat. 59: 2-20.

Atlar M, Unal B, Unal UO, Politis G, Martinelli E, Galli G, Davies C, Williams D. 2013. An experimental investigation of the frictional drag characteristics of nanostructured and fluorinated fouling-release coatings using an axisymmetric body. Biofouling. 29: 39-52.

Avnir D. 1995. Organic chemistry within ceramic matrices: doped sol-gel materials. Acc Chem Res. 28: 328 – 341.

Baier RE, Shafrin EG, Zisman WA. 1968. Adhesion: mechanisms that assist or impede it. Science. 162: 1360-8.

Baier RE, Meyer AE. 1992. Surface analysis of fouling-resistant marine coatings. Biofouling. 6: 165-180.

Banerjee I, Pangule RC, Kane RS. 2011. Antifouling coatings: Recent developments in the design of surfaces that prevent fouling by proteins, bacteria, and marine organisms. Adv Mater. 23: 690-718.

Bennett SM, Tang Y, McMaster D, Bright FV, Detty MR. 2008. Active-site/surface cooperativity in xerogel-sequestered selenoxide catalysts for the activation of hydrogen peroxide in an aqueous environment. J Org Chem. 73: 6849-6853.

Bennett SM, Finlay JA, Gunari N, Wells DD, Meyer AE, Walker GC, Callow ME, Callow JA, Bright FV, Detty MR. 2010. The role of surface energy and water wettability in aminoalkyl/fluorocarbon/hydrocarbon-modified xerogel surfaces in the control of marine biofouling. Biofouling. 26: 235-246.

Borghi V, Porte C. 2002. Organotin pollution in deep-sea fish from the Northwestern Mediterranean. Environ Sci Technol. 36: 4224-4228.

Brinker CJ, Scherer GW. 1990. Sol-gel science: the physics and chemistry of sol-gel processing. New York: Academic Press.

Callow ME, Callow JA, Pickett-Heaps JD, Wetherbee R. 1997. Primary adhesion of *Enteromorpha* (Chlorophyta, Ulvales) propagules: quantitative settlement studies and video microscopy. J Phycol. 33: 938–947.

Chambers LD, Stokes KR, Walsh FC, Wood RJK. 2006. Modern approaches to marine antifouling coatings. Surf Coat Technol. 201: 3642-3652.

Ciriminna R, Bright FV, Pagliaro M. 2015. Ecofriendly antifouling marine coatings. ACS Sustainable Chem Eng. 3: 559-565.

Clark CD, De Bruyn WJ, Jakubowski SD, Grant SB. 2008. Hydrogen peroxide production in marine bathing waters: implications for fecal indicator bacteria mortality. Mar Pollut Bull. 56: 397–401.

Cooper WJ, Zika RG. 1983. Photochemical formation of hydrogen peroxide in surface and ground waters exposed to sunlight. Science. 220: 771–712.

Dave BC, Soyez H, Miller JM, Dunn B, Valentine JS, Zink JI. 1995. Synthesis of protein-doped sol-gel SiO2 thin films: evidence for rotational mobility of encapsulated cytochrome c. Chem Mater. 7:1431 – 1434.

Detty MR, Ciriminna R, Bright FV, Pagliaro M. 2014. Environmentally benign sol-gel antifouling and foul-releasing coatings. Acc Chem Res. 47: 678-687.

Drabkova M. 2007. Selective effects of hydrogen peroxide on cyanobacteria photosynthesis. Photosynthetica. 45: 363–369.

Evariste E, Gatley CM, Detty MR, Callow ME, Callow JA. 2013. The performance of aminoalkyl/fluorocarbon/hydrocarbon-modified xerogel coatings against the marine alga *Ectocarpus crouaniorum*: relative roles of surface energy and charge. Biofouling. 29: 171-184.

Gatley CM, Muller LM, Lang MA, Alberto EE, Detty MR. 2015. Xerogel-sequestered silanated organochalcogenide catalysts for bromination with hydrogen peroxide and sodium bromide. Molecules. 20: 9616-9639.

Genovese S, Epifano F, Pelucchini C, Procopio A, Curini M. 2010. Ytterbium triflate catalyzed synthesis of chlorinated lactones. Tetrahedron Lett. 51: 5992-5995.

Goodman MA, Detty MR. 2004. Selenoxides as catalysts for the activation of hydrogen peroxide. Bromination of organic substrates with sodium bromide and hydrogen peroxide. Organometallics. 23: 3016-3020.

Gunari N, Brewer LH, Bennett SM, Sokolova A, Kraut ND, Finlay JA, Meyer AE, Walker GC, Wendt DE, Callow ME, Wendt DE, Callow ME, Callow JA, Bright FV, Detty MR. 2011. The control of marine biofouling on xerogel surfaces with nanometer-scale topography. Biofouling. 27:137–149.

Ingersoll CM, Bright FV. 1997. Using sol-gel-based platforms for chemical sensors. Chemtech. 27: 26 – 35.

Jack TR. 1999. Monitoring microbial fouling and corrosion problems in industrial systems. Corros Rev. 17: 1-31.

Le Bozec N, Compere C, L'Her M, Laouenan A, Costa D, Marcus P. 2001. Influence of stainless steel surface treatment on the oxygen reduction reaction in seawater. Corrosion Sci. 43: 765–786.

Lejars M, Margaillan A, Bressy C. 2012. Fouling release coatings: A nontoxic alternative to biocidal antifouling coatings. Chem Rev. 112: 4347-4390.

Martinelli E, Agostini S, Galli G, Chiellini E, Glisenti A, Pettit ME, Callow ME, Callow JA, Graf K, Bartels FW. 2008. The surface-segregate nanostructure of fluorinated copolymer-poly(dimethylsiloxane) blend films. Langmuir. 24:13138–13147.

McMaster DM, Bennett SM, Tang Y, Finlay JA, Kowalke GL, Nedved B, Bright FV, Callow ME, Callow JA, Wendt DE, Hadfield MG, Detty MR. 2009. Antifouling character of 'active' hybrid xerogel coatings with sequestered catalysts for the activation of hydrogen peroxide. Biofouling. 25: 21-33.

Mohammad A, Liebhafsky HA. 1934. The kinetics of the reduction of hydrogen peroxide by the halides. J Am Chem Soc. 56: 1680-1685.

Morey MS, Bryan JD, Schwarz S, Stucky GD. 2000. Pore surface functionalization of MCM-48 mesoporous silica with tungsten and molybdenum metal centers: perspectives on catalytic peroxide activation. Chem Mater. 12: 3435-3444.

Natalio F, Andre R, Hartog AF, Stoll B, Jochum KP, Wever R, Tremel W. 2012. Vanadium pentoxide nanoparticles mimic vanadium haloperoxidases and thwart biofilm formation. Nat Nanotechnol. 7: 530-535.

Owens DK, Wendt RC. 1969. Estimation of the surface free energy of polymers. J Appl Polym Sci 13: 1741-1747.

Pagliaro M, Ciriminna R, Palmisano G. 2009. Silica-based hybrid coatings. J Mater Chem. 19: 3116-3126.

Rosenhahn A, Schilp S, Kreuzer HJ, Grunze M. 2010. The role of "inert" surface chemistry in marine biofouling prevention. Phys Chem Chem Phys. 12: 4275-4286.

Schultz MP. 2007. Effects of coating roughness and biofouling on ship resistance and powering. Biofouling. 23: 331-341.

Schultz MP, Bendick JA, Holm ER, Hertel WM. 2011. Economic impact of biofouling on a naval surface ship. Biofouling. 27: 87-98.

Sokolova A, Cilz N, Daniels J, Stafslien SJ, Brewer LH, Wendt DE, Bright FV, Detty MR. 2012. A comparison of antifouling/foul-release characteristics of non-biocidal xerogel and commercial coatings toward micro- and macrofouling organisms. Biofouling. 28: 511-523.

Sokolova A, Bailey JJ, Brewer LH, Finlay JA, Fornalik J, Wendt DE, Callow ME, Callow JA, Bright FV, Detty MR. 2012a. Spontaneous multiscale phase separation within fluorinated xerogel coatings for fouling-release surfaces. Biofouling. 28: 143-157.

Tang Y, Finlay JA, Kowalke GL, Meyer AE, Bright FV, Callow ME, Callow JA, Wendt DE, Detty MR. 2005. Hybrid xerogel films as novel coatings for antifouling and fouling release. Biofouling. 21: 59-71.

Walker JV, Morey M, Carlsson M, Davidson A, Stucky GD, Butler A. 1997. Peroxidative halogenation catalyzed by transition-metal-ion-grafted mesoporous silicate materials. J Am Chem Soc. 119: 6921-6922.

Willey JD, Paerl HW, Go M. 1999. Impact of rainwater hydrogen peroxide on chlorophyll a content of surface Gulf Stream seawater off North Carolina, USA. Mar Ecol Prog Ser. 178: 145–150.

Williams SL, Schroeder SL 2004. Eradication of the invasive seaweed *Caulerpa taxifolia* by chlorine bleach. Mar Ecol Prog Ser. 272: 69–76.

Yuan J, Shiller AM. 2000. The variation of hydrogen peroxide in rain water over the South and Central Atlantic Ocean. Atm Environ. 34: 3973–3980.

Yuan J, Shiller AM. 2001. The distribution of hydrogen peroxide in the southern and central Atlantic Ocean. Deep Sea Res II. 48: 2947–2970.

Table 1: Contact angles and surface energies of xerogel coatings.

Composition /Name	100 TEOS	20:80 TTIP/TEOS	40:60 C8/TEOS	20:40:40 TTIP/C8/TEOS
Stored in Air				
Static Water Contact Angle ($\theta_{Ws}°$)	44 ± 2	45 ± 4	102.8 ± 0.6	99 ± 1
Static CH_2I_2 Contact Angle ($\theta_{(CH2I2)s}°$)	46 ± 2	37 ± 1	69 ± 1	66 ± 1
Total Surface Energy γ_S (mN m-1)	56 ± 2	57 ± 2	23.2 ± 0.2	25.0 ± 0.1
Immersed 24 h in ASW Water				
Static Water Contact Angle ($\theta_{Ws}°$)	31 ± 1	35 ± 4	99.4 ± 0.8	94 ± 2
Static CH_2I_2 Contact Angle ($\theta_{(CH2I2)s}°$)	47 ± 1	40 ± 2	65 ± 1	63 ± 1
Total Surface Energy γ_S (mN m^{-1})	63.9 ± 0.6	62 ± 2	26 ± 1	27 ± 1

[a] Values are the average of 3 replicate runs (6 measurements).[a] Error limits are ± one standard deviation.

Table 2. Rates of halogenation of 4-pentenoic acid (1) with H_2O_2 and sodium halide salts at pH 7 or pH 8 and 298 ± 1 K in the presence of xerogel catalysts.

entry	Xerogel	Ti, mole-%	pH	k_{obs}, s^{-1}	k_{rel}
			Bromination		
1	100 TEOS	0	7.0	$(2.47 \pm 0.15) \times 10^{-7}$ [a]	1
2	20:80 TTIP/TEOS	3.5	7.0	$(8.44 \pm 0.10) \times 10^{-5}$ [a]	340
3	40:60 C8/TEOS	0	7.0	$(5.94 \pm 0.05) \times 10^{-7}$ [a]	2.4
4	20:40:40 TTIP/C8/TEOS	3.5	7.0	$(3.37 \pm 0.09) \times 10^{-6}$ [a]	14
5	100 TEOS	0	8.0	$(7.34 \pm 0.44) \times 10^{-7}$ [a]	3
6	20:40:40 TTIP/C8/TEOS	3.5	8.0	$(1.36 \pm 0.11) \times 10^{-6}$ [a]	5.5
			Chlorination		
5	100 TEOS	0	7.0	$(1.48 \pm 0.27) \times 10^{-7}$ [b]	1
7	20:80 TTIP/TEOS	60	7.0	$(1.51 \pm 0.05) \times 10^{-5}$ [a]	100
8	40:60 C8/TEOS	0	7.0	$(2.00 \pm 0.11) \times 10^{-7}$ [a]	1.4
9	20:40:40 TTIP/C8/TEOS	20	7.0	$(1.03 \pm 0.05) \times 10^{-6}$ [a]	5.4
10	20:40:40 TTIP/C8/TEOS	60	7.0	$(3.22 \pm 0.62) \times 10^{-6}$ [b]	22
6	100 TEOS	0	8.0	$(7.20 \pm 0.39) \times 10^{-8}$ [b]	0.5
11	20:40:40 TTIP/C8/TEOS	60	8.0	$(1.46 \pm 0.65) \times 10^{-6}$ [b]	9.9

[a] Values are the average of duplicate runs. Error limits are ± one half of the range. [b] Values are the average of triplicate runs. Error limits are ± one standard deviation.

Figure Captions

Figure 1. SEM images of the TTIP/C8/TEOS xerogel a) from above and b) along an edge stored in air and c) from above and d) along an edge post-immersion in ASW.

Figure 2. Changes in the TTIP/C8/TEOS xerogel pre- and post-immersion in DI water or 200 μM H_2O_2 as determined by XPS. Mean of four independent measurements for coatings either pre-immersion or post-immersion for 24 in DI water or 24 h in 200 μM H_2O_2. Error bars represent 1 SD for the four independent measurements for the three conditions.

Figure 3. a) Rate of bromination of **1** (ln [A] vs. time, where A is the concentration of **1**) with 1.4 M NaBr and 0.21 M H_2O_2 comparing the TTIP/TEOS (filled circles), TTIP/C8/TEOS (Filled triangles), and TEOS xerogels (open circles) as catalysts at 298 ± 1 K at pH 7 or b) at pH 8. All points represent the average of duplicate runs and error bars represent the range of values. C) Rate of chlorination of **1** with 2.7 M NaCl and 0.68 M H_2O_2 comparing the TTIP/TEOS (filled circles), TTIP/C8/TEOS (Filled triangles), and TEOS xerogels (open circles) as catalysts at pH 7 or d) at pH 8. All reactions were run at 298 ± 1 K. All points represent the average of triplicate runs and error bars represent ± 1 SD.

Figure 4. Halogenation of 50 μM phenol red in ASW a) via the incremental addition of bleach (HOCl) to give the equivalent of the concentrations shown with b) an expansion of the 400-450-nm region or c) via the addition of 50 μM H_2O_2 in the glass cuvette coated with the TTIP/C8/TEOS xerogel with d) an expansion of the 400-450-nm region. The inset of a) shows a plot of the initial absorbance at 434 nm minus the absorbance at time, *t*, plotted against the equivalent concentration of bleach. The slope of the line gives the change in absorbance per μM bleach.

Figure 5. The density of attached spores on C8/TEOS and TTIP/C8/TEOS coatings after 45-min settlement time in the presence of different concentrations of H_2O_2. Each point is the mean from 90 counts on 3 replicate slides. Bars show 95% confidence limits. Values of the bars that share a letter are not significantly different ($p > 0.05$) from one another.

Figure 6. a) Biomass of sporelings on C8/TEOS and TTIP/C8/TEOS coatings after 7 d. Each point is the mean biomass from 6 replicate slides measured using a fluorescence plate reader (RFU; relative fluorescence unit). b) Percent removal of 7-day-old sporelings from coatings due to an impact pressure of 30 kPa. Each point is the mean removal of biomass from 6 replicate slides measured using a fluorescence plate reader. Bars show standard error of the mean determined from arcsine transformed data. Values of the bars that share a letter are not significantly different ($p > 0.05$) from one another.

Figure 7. The impact of sodium hypochlorite on the settlement of zoospores and growth of sporelings of *U. linza*. a) The density of attached spores after 45-min settlement time in the presence of a range of concentrations of sodium hypochlorite. Each point is the mean from 90 counts on 3 replicate slides. b) The biomass of sporelings after 7-days growth in the presence of sodium hypochlorite. Each point is the mean biomass from 4 replicate wells measured using extracted chlorophyll in a fluorescence plate reader (RFU; relative fluorescence unit). Bars show 95% confidence limits.

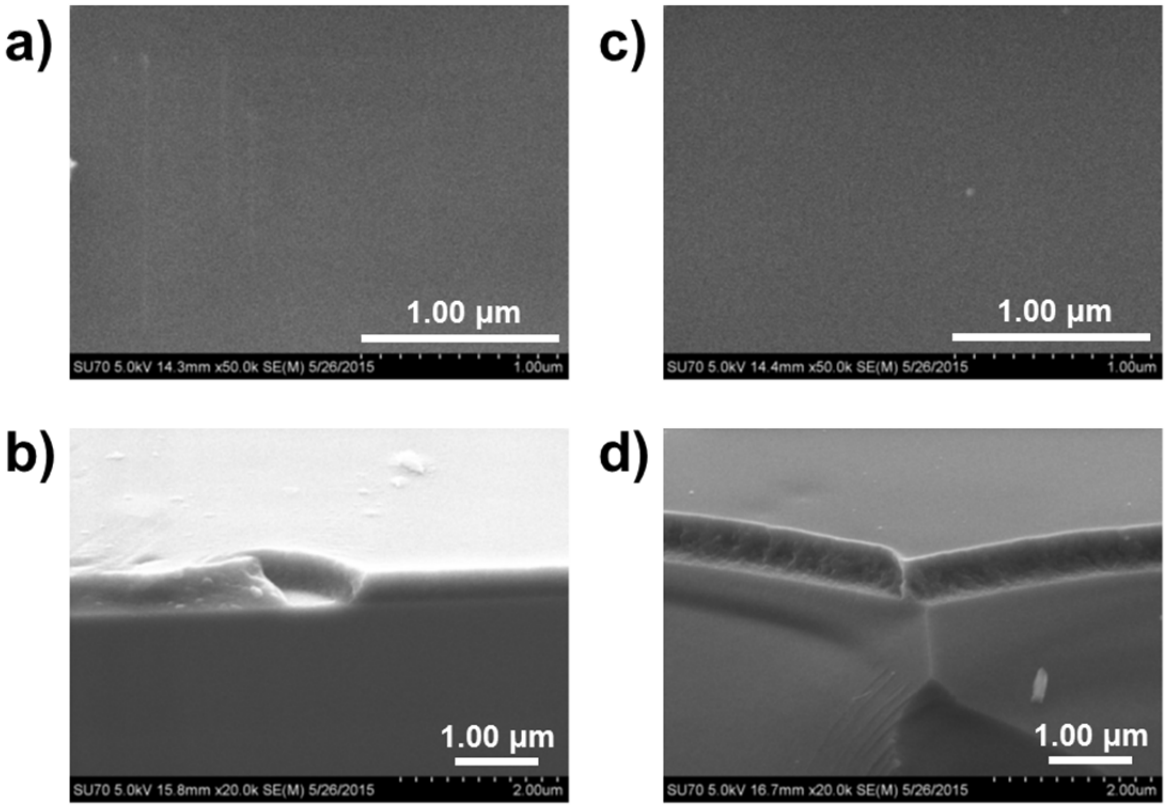

Figure 1. SEM images of the TTIP/C8/TEOS xerogel a) from above and b) along an edge stored in air and c) from above and d) along an edge post-immersion in ASW.

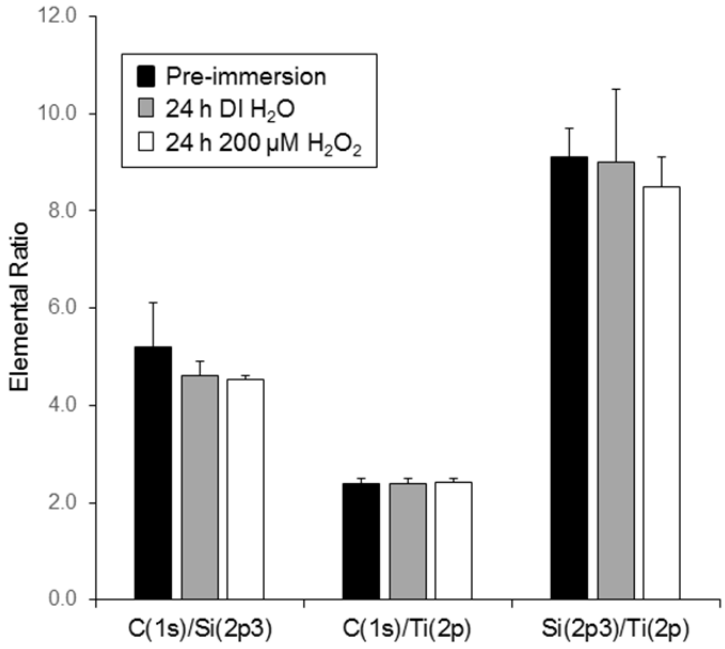

Figure 2. Changes in the TTIP/C8/TEOS xerogel pre- and post-immersion in DI water or 200 μM H_2O_2 as determined by XPS. Mean of four independent measurements for coatings either pre-immersion or post-immersion for 24 in DI water or 24 h in 200 μM H_2O_2. Error bars represent 1 SD for the four independent measurements for the three conditions.

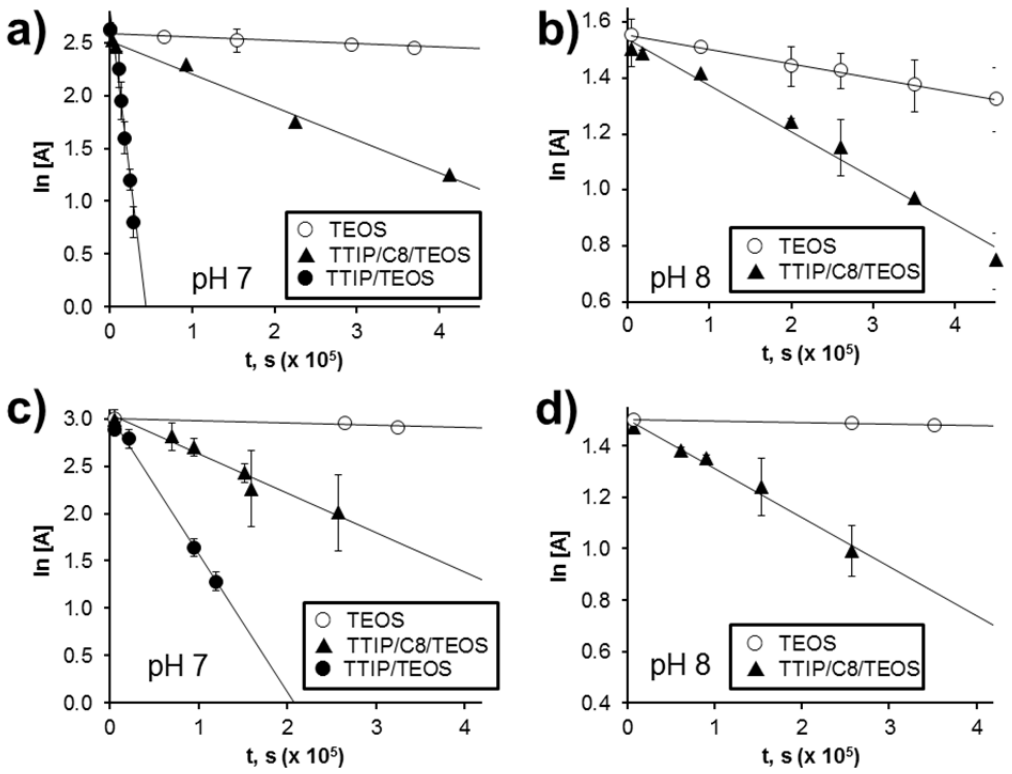

Figure 3. a) Rate of bromination of **1** (ln [A] vs. time, where A is the concentration of **1**) with 1.4 M NaBr and 0.21 M H_2O_2 comparing the TTIP/TEOS (filled circles), TTIP/C8/TEOS (Filled triangles), and TEOS xerogels (open circles) as catalysts at 298 ± 1 K at pH 7 or b) at pH 8. All points represent the average of duplicate runs and error bars represent the range of values. C) Rate of chlorination of **1** with 2.7 M NaCl and 0.68 M H_2O_2 comparing the TTIP/TEOS (filled circles), TTIP/C8/TEOS (Filled triangles), and TEOS xerogels (open circles) as catalysts at pH 7 or d) at pH 8. All reactions were run at 298 ± 1 K. All points represent the average of triplicate runs and error bars represent ± 1 SD.

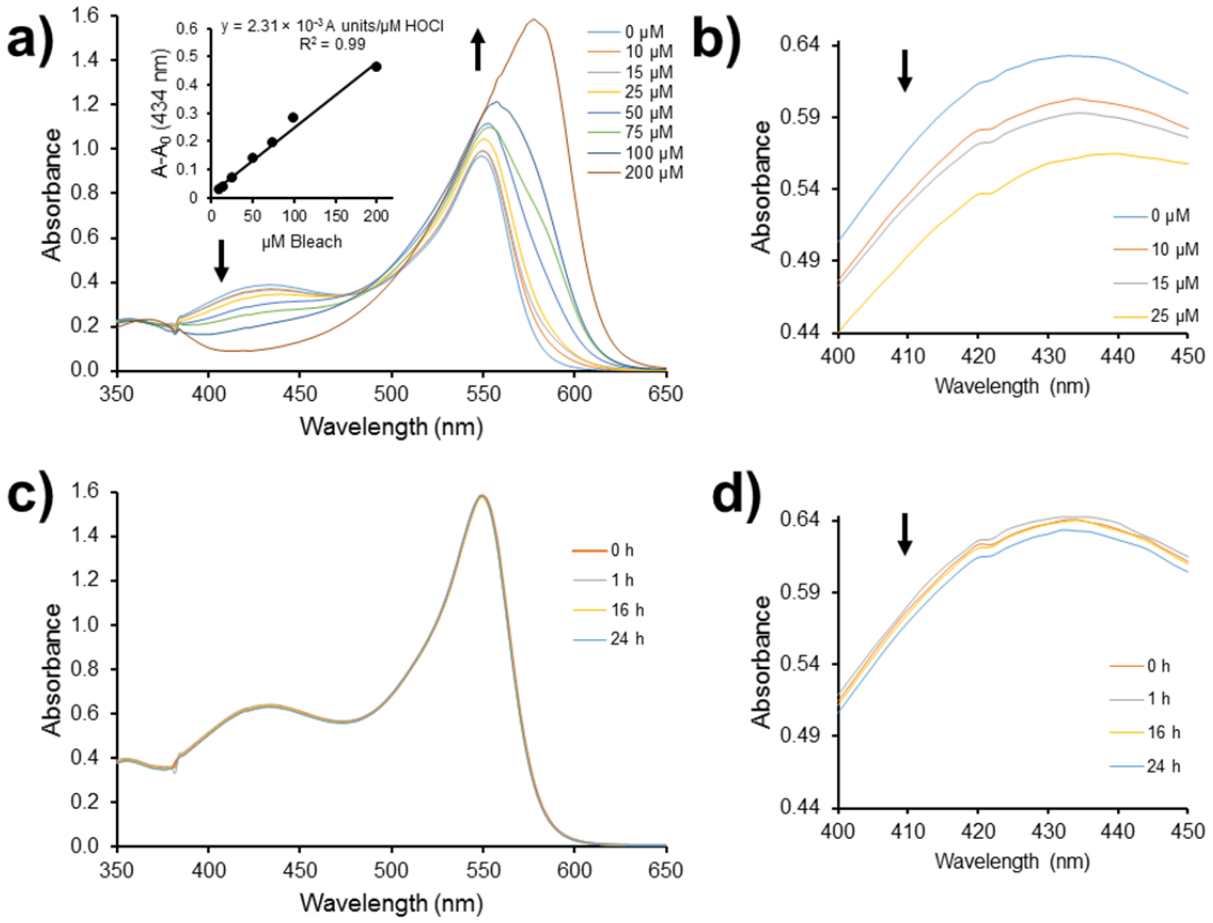

Figure 4. Halogenation of 50 μM phenol red in ASW a) via the incremental addition of bleach (HOCl) to give the equivalent of the concentrations shown with b) an expansion of the 400-450-nm region or c) via the addition of 50 μM H_2O_2 in the glass cuvette coated with the TTIP/C8/TEOS xerogel with d) an expansion of the 400-450-nm region. The inset of a) shows a plot of the initial absorbance at 434 nm minus the absorbance at time, *t*, plotted against the equivalent concentration of bleach. The slope of the line gives the change in absorbance per μM bleach.

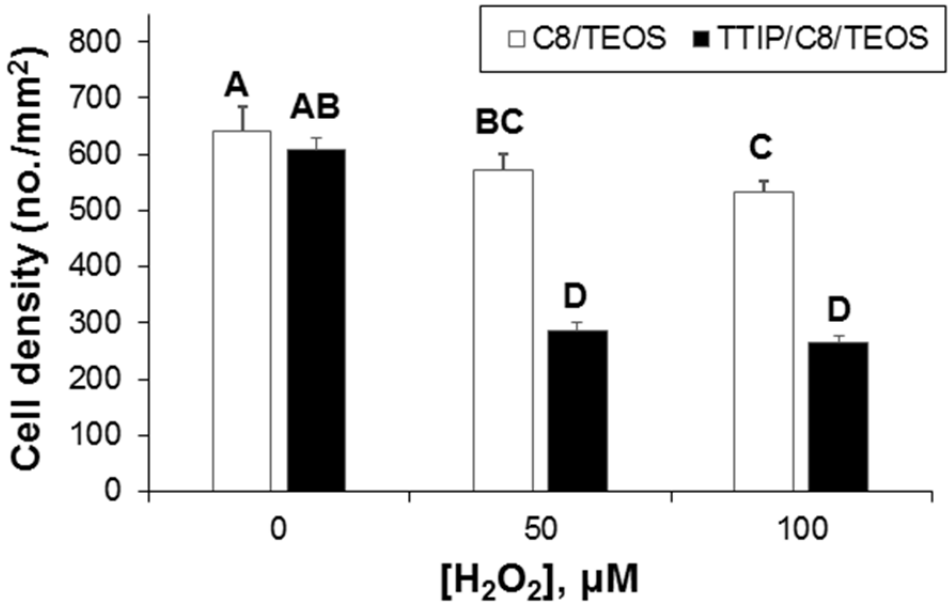

Figure 5. The density of attached spores on C8/TEOS and TTIP/C8/TEOS coatings after 45-min settlement time in the presence of different concentrations of H_2O_2. Each point is the mean from 90 counts on 3 replicate slides. Bars show 95% confidence limits. Values of the bars that share a letter are not significantly different ($p > 0.05$) from one another.

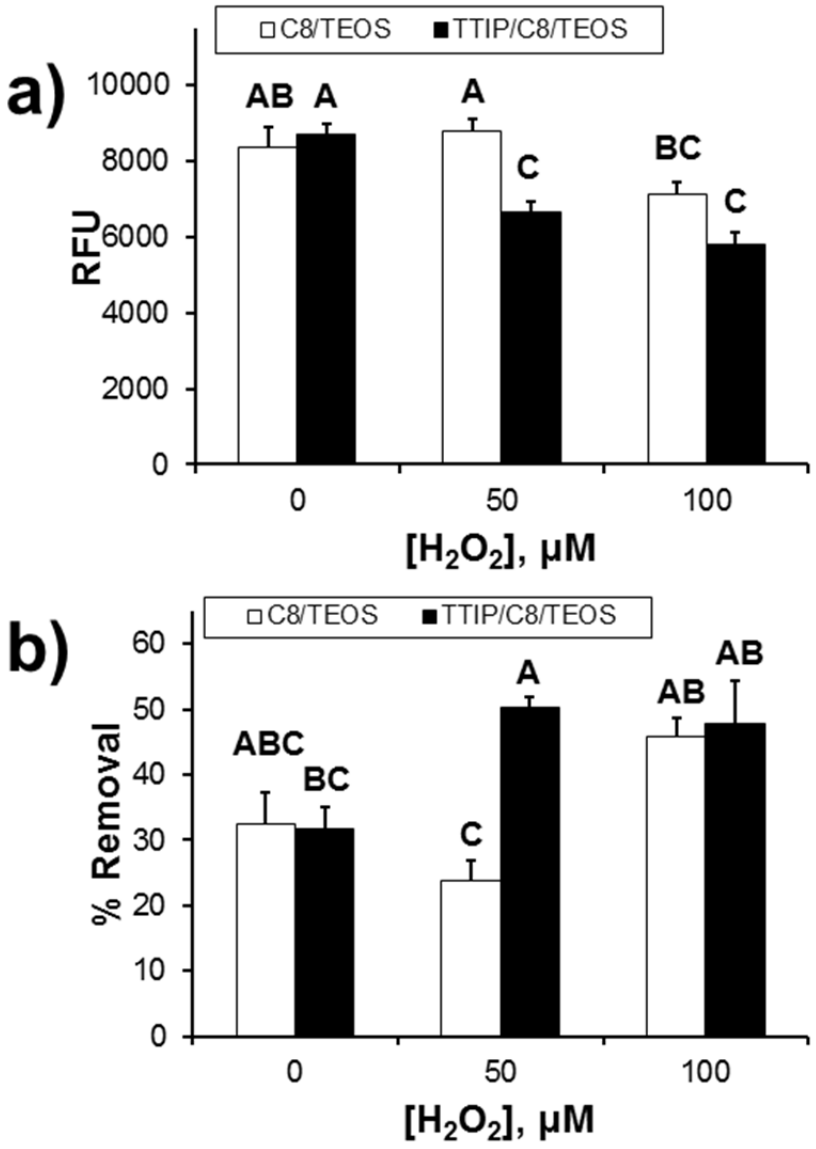

Figure 6. a) Biomass of sporelings on C8/TEOS and TTIP/C8/TEOS coatings after 7 d. Each point is the mean biomass from 6 replicate slides measured using a fluorescence plate reader (RFU; relative fluorescence unit). b) Percent removal of 7-day-old sporelings from coatings due to an impact pressure of 30 kPa. Each point is the mean removal of biomass from 6 replicate slides measured using a fluorescence plate reader. Bars show standard error of the mean determined from arcsine transformed data. Values of the bars that share a letter are not significantly different ($p > 0.05$) from one another.

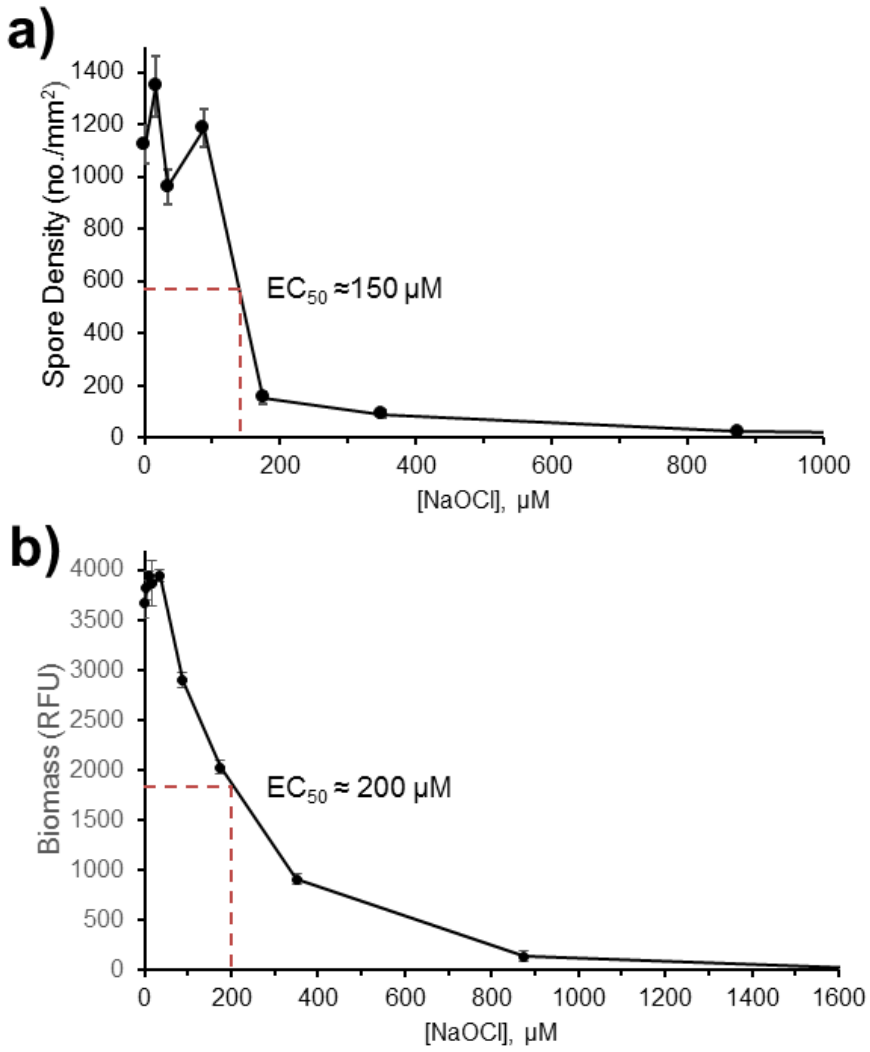

Figure 7. The impact of sodium hypochlorite on the settlement of zoospores and growth of sporelings of *U. linza*. a) The density of attached spores after 45-min settlement time in the presence of a range of concentrations of sodium hypochlorite. Each point is the mean from 90 counts on 3 replicate slides. b) The biomass of sporelings after 7-days growth in the presence of sodium hypochlorite. Each point is the mean biomass from 4 replicate wells measured using extracted chlorophyll in a fluorescence plate reader (RFU; relative fluorescence unit). Bars show 95% confidence limits.